



Inorganic and organic smectite for synthetic and real textile water treatment. Optical and luminescence properties

Fadhila Ayari*, Malika Trabelsi Ayadi

Laboratory Applications of Chemical Resources, Natural Substances and Environment (LACReSNE), Faculty of Sciences of Bizerte, University of Carthage, Tunisia, Tel. +21621791747, email: fadhilaayari@yahoo.fr (F. Ayari), malikatrabelsi_ayadi@yahoo.fr (M.T. Ayadi)

Received 25 January 2018; Accepted 1 September 2018

ABSTRACT

Surfactant modified smectite was prepared using hexadecyltrimethylammonium bromide at three cation exchange capacity (CEC) levels. Obtained organosmectites labeled H₁-Sm (I = 1, 2 and 3 CEC) were characterized by several methods. Results show that the point of zero charge (PZC) of organo-modified smectite was displaced to the basic zone compared to that of Na-smectite. Hybrid material develops more positives surface charges, a heterogeneous structure with a great basal spacing layer. H₃-Sm and purified smectite (Arp) were then tested as adsorbents for the removal of an anionic diazo dye. Amount of dye removal by H₃-Sm (100%) was found to be around ~3 times higher than that of Arp. Complexed organosmectite after Congo Red (CR) dye adsorption can be used in photocatalytic field. The treated textile effluent by Arp, collected from textile Tunisian industry, can be re-used for vegetation irrigation, adapted to high salinity

Keywords: Organoclay; Anionic dye; Adsorption isotherms; Textile effluent; Modeling

1. Introduction

Extensive use of colorants resulted in their frequent detection in wastewater streams. However, current methods relying on activated sludge systems for the removal of color arising from the presence of the water-soluble reactive dyes are inadequate, both at on-site installations and even after dilution with domestic wastewater at sewage works [1,2]. Many conventional physico-chemical methods employed for the treatment of textile industry effluents, such as, biological process [3], chemical oxidation [4], coagulation [5], adsorption [6–9]. But, they stay inefficient due to either expensive cost, or generation of concentrated sludge, and/or difficulty of treating a large volume of wastewater.

Among these techniques, adsorption process who is largely used in water and wastewater treatment because of its simplicity, low-cost of operation and wide end-use applications according to Onyango et al. [10]. Various adsorbents have been tested in the removal of dye from textile effluent,

including commercial activated carbons, has been proved to be simple, more efficient and economically feasible technique [11]. However, the high cost of activated carbon [12] and its regeneration associated problems has led to the development of alternative adsorbents, which are cheaper, easy to regenerate and can be disposed of safely.

In the last few years, numbers of low cost adsorbents for wastewater treatment and various dyes removal have been reported such as bentonite [13], sepiolite [14] and kaolinite [15]. Among these, natural clays were explored as low-cost alternative and effective adsorbents for the textile dyes removal from wastewater.

Clay belong to smectite family, have been widely used in a range of applications because of their high cation exchange capacity, swelling capacity, high specific surface area, and consequential strong adsorption capacity as described in these works [16,17]. But, natural smectite are ineffective sorbents for the nonpolar, nonionic and anionic organic compounds in water because of their hydrophilic property due to hydration of metal ions Juang et al. [16]. Surface properties of natural bentonite can be significantly

*Corresponding author.

modified with alkylammonium surfactants, by simple ion-exchange reactions [18], assured by Coulombic interaction between organic surfactant cations and the adsorbent according to Ozcan et al. [19]. This modification converts the surface properties from highly hydrophilic/lipophobic to increasingly hydrophobic/lipophilic as confirmed in these studies [16,20]. Cationic surfactant greatly increases the interlayer spaces, occupy the exchange sites of bentonite clay and hence the surface area is increased as reported in the study of Ozcan et al. [19].

Such changes are important for the application of organoclays and their significance in hydrophobic organoclays is highlighted by their use for a wide variety of environmental application [18].

Organosmectite becomes more effective adsorbent, it can be used as a filter material for air purification from benzene [21], as the transport of nonionic contaminants in ground water [22] as rheological control agents [23] and electric materials [24].

As contribution to the objectives of sustainable treatment of wastewaters, this study aims to characterize a locally Tunisian clay before and after modification with cationic surfactant and to investigate their suitability as adsorbents for anionic dye and textile effluent containing anionic dye.

Hence, hexadecyltrimethylammonium bromide (HDTMA) surfactant was used, as a model of a long alkyl cationic surfactant, for the preparation of organoclays.

Adsorption experiments were carried out under various parameters, kinetics characteristics of the adsorption were pointed out and modeling results were examined to identify the mechanisms of interaction. Congo red (CR) was chosen as anionic dye in this research.

2. Materials and method

2.1. Chemicals and materials

2.1.1. Raw material

Clay sample employed in the present study was provided from a deposit located at "Kef Abbed" north of Tunisia. This clay is a natural Ca^{2+} -smectite associated with kaolinite and with quartz and calcite as impurities.

2.1.2. Preparation of purified clay

In order to remove these impurities from the clay fraction and to obtain purified clay, the $<2 \mu\text{m}$ size fraction of the raw clay (Arb) was purified, using the classic method [25], by repeated cation exchange in NaCl (1 M) followed by washing, sedimentation and dialysis operations in order to ensure almost complete substitution of interlayer ions with sodium.

The purified clay (Arp) is finally dried at 70°C and then crushed and sieved.

2.1.3. Model pollutant

Dye used in this investigation is Congo red (denoted as CR, $\text{C}_{32}\text{H}_{22}\text{N}_6\text{Na}_2\text{O}_6\text{S}_2$, FW: 696.66), from Segma-Aldrich, used without any further purification. It is a synthetic

diazo anionic direct dye, which contain chromophoric groups. The IUPAC name of CR is [1-naphthalene sulfonic acid, 3,3 - (4,4 -biphenylene bis (azo)) bis (4-amino-) disodium salt.

Congo red contains $-\text{NH}_2$ and $-\text{SO}_3$ functional groups (Fig. 1c). The CR sodium salt is responsible for dyeing cotton full red and is the first synthetic dye able of directly dyeing cotton [26]. It has a strong affinity for cellulose fibers, very used in textile dyeing industry.

CR is very sensitive to the pH and would change from red to blue, due to $\Pi - \Pi^*$ transition in azo group shift to higher wavelength because of protonation. This experiment revealed that at lower pH it becomes cationic and shows two tautomeric forms of protonated CR, i.e. ammonium rich variety and azonium variety [27].

In order to determine experimentally the reliable λ_{max} value for CR dye at desired pH experiments were carried out over a pH range of 3–7 (Mettler Toledo Seven Easy S20K pH meter), and then the UV–vis absorption spectra of the solutions were recorded with a UV–vis spectrophotometer (Fig. 1b). pKa of CR was also determined, it found equal 3.7 (Fig. 1a).

2.2. Preparation of organoclays

Surfactant used in this study for the organoclays complexes is hexadecyltrimethylammonium bromide (Fig. 2) denoted as HDTMA ($\text{C}_{19}\text{H}_{42}\text{NBr}$, FW: 364.45) from Segma-Aldrich, used without any further purification. It is a cationic surfactant with micelle concentration (CMC) of 0.9 mM.

To prepare organoclay, twenty grams of the Na-saturated clay (Arp) was dispersed in 400 mL of distilled water with a Heidolph magnetic stirrer for about 1 h. A stoichiometric amount of the surfactant was dispersed in 100 mL of distilled water and stirred for 30 min. The dissolved surfactant was slowly added to the clay suspension at 80°C . The CEC of Arp was 89 meq/100 g, which represents a measure of the loading of the clay with the cationic surfactant. For instance 1.0 CEC correlates with the addition of 89 meq cation per 100 g of Arp intercalated into the Arp. During the synthesis, a range of surfactant loading in terms of the CEC value from 1.0 CEC through 3.0 CEC was prepared and labeled H_1 , H_2 and H_3 respectively. The mixtures were stirred for 24 h at 80°C using a Heidolph magnetic stirrer. All organoclays products were washed several times and then dialyses successively with distilled water until there were no free bromide anions (as determined by the use of the AgNO_3), centrifuged and dried in an oven at 70°C . The dried organoclays were ground in an agate mortar and stored in vacuum desiccators for 7 d.

Organoclay prepared at a surfactant concentration of 1.0 CEC was marked as $\text{H}_1\text{-Sm}$ and the others were marked in a similar fashion ($\text{H}_2\text{-Sm}$ and $\text{H}_3\text{-Sm}$).

2.3. Instrumentation and methods of characterization of adsorbents

2.3.1 X-ray diffraction (XRD)

The raw and purified clay, the synthesized organosmectites and adsorbents after adsorption of CR were character-

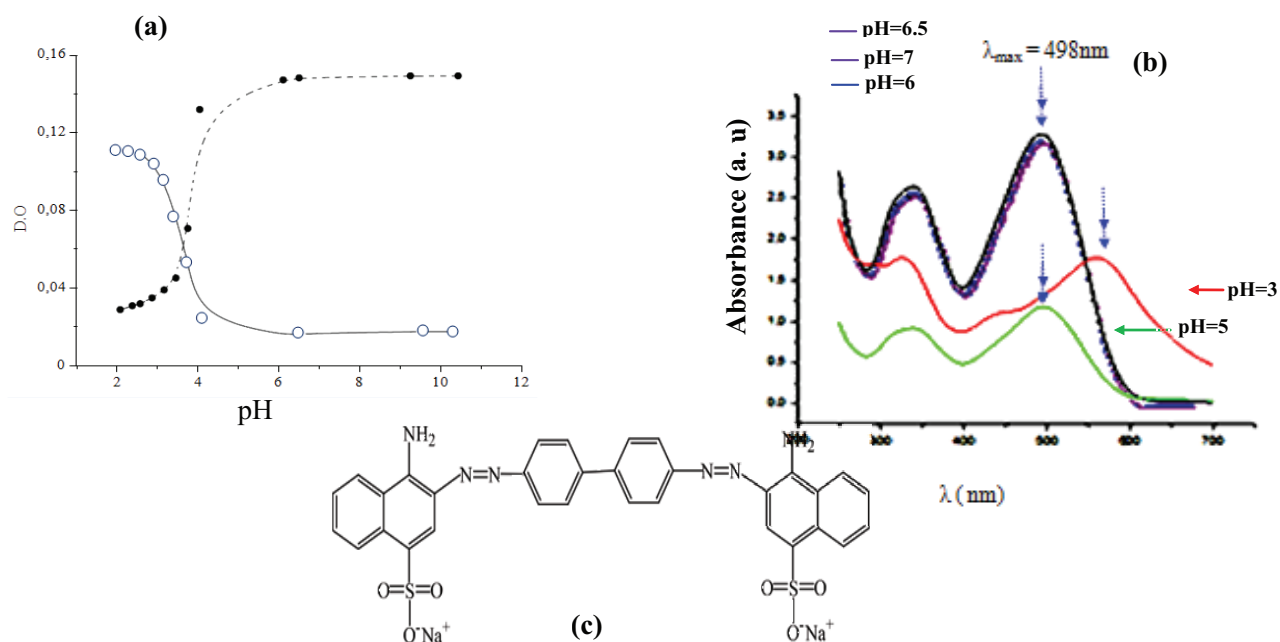


Fig. 1. (a) CR pka determination, (b) CR λ_{\max} value, (c) Chemical structure of Congo red (pH > 5.5).

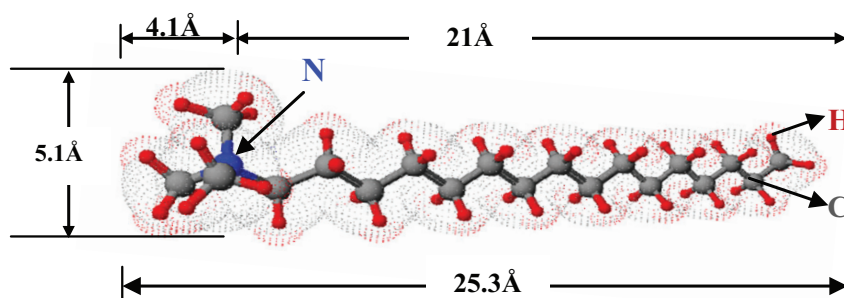


Fig. 2. Chemical structure of HDTMA.

ized by X-ray diffraction. Powdered XRD were recorded using Cu K α radiation ($\lambda = 1.54 \text{ \AA}$) on a Philips PAN analytical X'pert PRO diffractometer operating at 40 KV and 40 mA between 5° and 35° (2θ). For XRD at low angle section it was between 1.5° and 8° (2θ).

2.3.2. Transmission electron microscopy (TEM)

Pure (Arp) and organoclay (H₃-Sm) ultrasonically dispersed in absolute ethanol solution and a small drop of each mixers suspension was prepared on carbon-coated films and dried in an oven at 60°C for TEM studies. Microstructure of these two samples was performed via FEI Tecnai G20 transmission electron.

2.3.3. Brunauer Emmett and Teller (BET)

The specific surface areas, pore volumes of raw, pure, and organoclays were measured using the physical adsorption of nitrogen by Quantachrome Autosorb-1 instrument. The samples were out gassed overnight under nitrogen. Specific sur-

face areas were determined with the Brunauer-Emmett-Teller (BET) equation using nitrogen as the adsorbate.

2.3.4. Cation exchange capacity (CEC)

CEC was determined using the copper ethylenediamine ((EDA)₂CuCl₂) complex [28] the CEC was determined from the amount of Cu(EDA)_2^{2+} adsorbed by the adsorbent.

2.3.5. Point of zero proton charge (PZC) of Na-clay and organosmectites

2.3.5.1. Mass titration

Point of zero proton charge (PZC) was estimated according to Noh and Schwarz; [29] Approximately 0.1 g of dry clay was added to 50 mL of 0.1 M NaCl solution at different pH values, pH was recorded after an equilibrium time. Then, a new amount of sample was introduced which induced a change in the pH solution. This procedure was repeated until the pH was stable after sample

addition. This was the pH where proton adsorption was zero (PZC).

2.3.6. Optical properties

The optical properties of the studied materials were investigated by UV-Vis diffuse reflectance spectroscopy (DRS) using UV-Vis spectrophotometer (Shimadzu UV-2700).

Time-resolved photoluminescence (PL) was performed on a FLS980 spectrometer by applying laser excitation at 498 nm.

2.4. Adsorption experiments

The adsorption of CR onto Arp and H₃-Sm adsorbents was studied in aqueous solution in a batch system. Stock solution (S₁) of 69.66 mg L⁻¹ of CR was prepared, at natural pH (6.2), by dissolving appropriate amount of CR in distilled water and the concentrations that had been used are obtained by dilution of S₁.

100 mg of the adsorbent were dispersed in 50 mL of CR solution. The concentration of CR in solution was typically in the range of 13.93–69.66 mg L⁻¹ (69.66 mg L⁻¹ for the adsorption study and 13.93–69.66 mg L⁻¹ for the isotherm study). The mixture was continuously agitated on a shaker for 60 min at room temperature. After shaken the mixture was centrifuged at 4500 rpm for 20 min and the supernatants were analyzed by UV-Vis spectrophotometer at λ_{max} (498 nm). The amount of dye adsorbed on Arp and H₃-Sm, q_e (mg·g⁻¹), was calculated by the following relationship:

$$q_e = \frac{(C_0 - C_e) \cdot V}{m} \quad (1)$$

where C₀ and C_e (mg·L⁻¹) are the initial and equilibrium dye concentration respectively, V is the volume of the solution (L), and m is the amount of the adsorbent (g).

Kinetic studies was investigated as follows, 100 mg of the adsorbent were added to 50 mL of CR solution (69.66 mg L⁻¹) at neutral pH (6.2). The dispersions were shaken under agitation speed of 400 rpm for a contact time varying from 10 min to 120 min. After each time of contact the mixture was centrifuged and the supernatants were analyzed. The dye uptake by the adsorbents was calculated by the following equation:

$$q_t = \frac{(C_0 - C_t) \cdot V}{m} \quad (2)$$

where q_t (mg·g⁻¹) is the amount of CR adsorbed at time t, V is the volume of the solution (L), C₀ and C_t are the initial and at time t dye concentration respectively and m is the amount of the adsorbent (g).

The final pH of each solution was measured and it was found that the pH changes during the adsorption experiments were negligible. Each experiment was performed three times, and the experimental results were the average value.

The effect of adsorbents dose onto the removal of CR from aqueous solution was investigated. 50 mL of CR solution was added to an amount of adsorbent, varied from

0.1 g to 1 g, the mixture was stirred until equilibrium was reached, then centrifuged and the supernatant was analyzed by UV-Vis spectrometer at λ_{max}. The CR removal efficiency percentage (R%) was calculated by the following equation:

$$R = \frac{(C_0 - C_e)}{C_0} \times 100 \quad (3)$$

2.5. Equilibrium isotherm modeling

2.5.1. Langmuir model

The Langmuir isotherm [30] assumes monolayer adsorption on a uniform surface with a finite number of adsorption sites. Once a site is occupied, no further sorption can take place at that site, the surface will eventually reach a saturation point where the maximum adsorption of the surface will be achieved. The linear form of the Langmuir isotherm model is given by the following equation:

$$\frac{C_e}{q_e} = \frac{1}{K_L q_m} + \frac{C_e}{q_m} \quad (4)$$

where K_L is the Langmuir constant adsorption (L·mg⁻¹) related to the free energy of adsorption

2.5.2. Freundlich model

Freundlich model is based on the assumption that the adsorption take place on heterogeneous surface [31]. The linear form of Freundlich equation is given as follows:

$$\ln q_e = \frac{1}{n} \ln C_e + \ln K_f \quad (5)$$

where k_f and n are the Freundlich adsorption isotherm constants indicated the capacity and the intensity of the adsorption respectively.

3. Result and discussion

3.1. Characterizations of adsorbents

3.1.1. Chemical composition

Mineralogical composition of the raw (Arb) and purified sample (Arp) is reported in Table 1. Results suggest the presence of silica and alumina as major constituents with traces of potassium, magnesium and calcium oxides.

3.1.2. X-ray diffraction

XRD patterns of Arb and Arp (Fig. 3), shows the appearance of peaks at 14.7 Å on the raw sample which decreased to 12.26 Å after purification, confirms the presence of smectite. Peaks at 7.01 Å and 3.52 Å suggested the presence of kaolinite. Presence of Illite fraction was confirmed by a peak at 2.88 Å. Peaks at 4.25 Å and 3.32 Å marked the presence of quartz, peak at 3.01 Å is related to carbonate. Quartz and carbonate, considered as impurities [32], disappear after purification.

Table 1
Chemical composition (w%)

| % M _x O Sample | Arp | Arb |
|--------------------------------|-------|-------|
| SiO ₂ | 50.8 | 40.96 |
| MgO | 3.95 | 3.43 |
| CaO | 0.28 | 16 |
| Fe ₂ O ₃ | 6 | 5.09 |
| Al ₂ O ₃ | 17.4 | 9.23 |
| Na ₂ O | 1.39 | 1.46 |
| K ₂ O | 0.84 | 0.43 |
| LOI | 20.31 | 22.5 |

LOI: loss of ignition

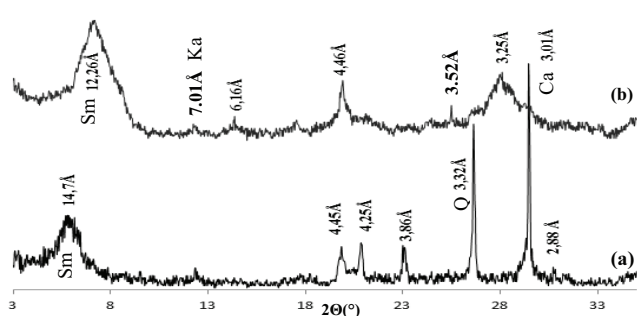


Fig. 3. XRD patterns of Arb (a) and Arp (b).

Fig. 4 shows the X-ray diffraction patterns of Arp and organosmectites prepared at different surfactant loading (H₁-Sm, H₂-Sm and H₃-Sm). Results show that d₀₀₁ of Arp (12.26 Å) increase gradually (26.2 Å → 32 Å → 42.2 Å) with the increase of surfactant concentrations. The basal spacing values provide the intercalation and molecular structure configuration of the organic surfactant into the interlayer space of clay depending on the ratio of surfactant loading [33–35]. The increase in basal spacing of Arp with HDTMA cations can be attributed to the replacement of the inorganic layer cations and their hydration water with HDTMA cations.

The arrangements of the surfactant molecules in the interlayer region can be distinguished by comparing the interlayer expansions Δd (Δd = d₀₀₁ - 9.6, the thickness of phyllosilicates layer belong to smectite group is 9.6 Å) and molecular dimension of the surfactant (Fig. 2) [16,36,37]. Results of surfactant arrangement in the interlayer space were summarized in Table 2.

X-ray diffraction patterns of the hybrid samples show the appearance of extended peaks that may imply the coexisting of several phases by the progression of transformation of the arrangement models of HDTMA⁺ ion.

H₃-Sm, prepared at the highest surfactant loading (3 CEC), shows the appearance of two different values of basal space one at 42.2 Å and the second at 32 Å which signify that there are two phases in this sample related to a PB and a PM surfactant arrangement (Table 2). This result differs from other previous work [38,40] which gives only

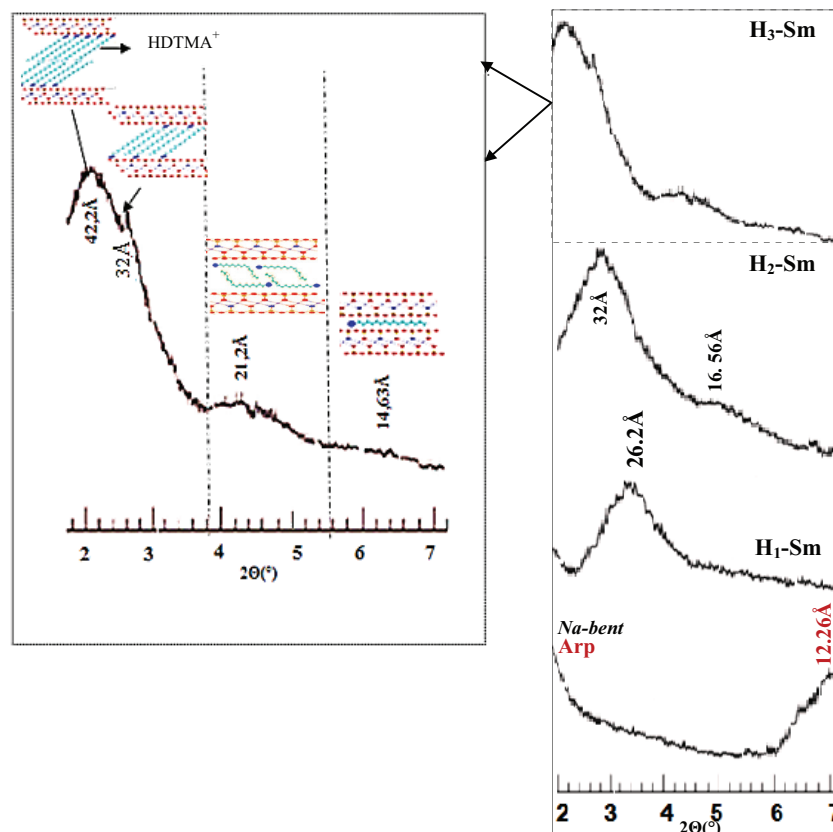


Fig. 4. XRD patterns of Na-smectite (Arp) and organosmectites prepared at different HDTMA⁺ concentrations.

Table 2
Surfactant arrangement type obtained in this study compared with previous data

| Samples | d_{001} (Å) | Surfactant arrangement type | References |
|--------------------|-----------------|-----------------------------|------------|
| H ₁ -Sm | d_{001} 26.2 | Parafine monolayer (PM) | [38,36] |
| H ₂ -Sm | d_{001} 32 | Paraffin monolayer (PM) | [38,40] |
| | d_{002} 16.56 | Lateral bilayer (LB) | |
| H ₃ -Sm | d_{001} 42.2 | Paraffin-type bilayer (PB) | This work |
| | 32 | Paraffin monolayer (PM) | |
| | d_{002} 21.2 | Pseudo-trilayer (PT) | [34,39] |
| | d_{003} 14.63 | Lateral-monolayer (LM) | [35] |

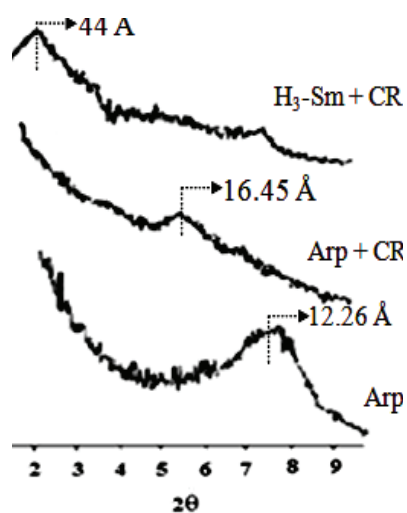


Fig. 5. XRD patterns of Arp and H₃-Sm after CR adsorption.

homostructure samples. H₃-Sm presents a heterogeneous structure.

The XRD patterns of Arp and H₃-Sm after CR adsorption (Fig. 5) shows an increase in the basal space of each adsorbent which suggested the penetration of CR onto the interlayer space.

3.1.3 TEM

Analysis of Arp and H₃-Sm by MET (Fig. 6) confirms perfectly the results found by X-ray diffraction. Results reveal the existences of layer expanded at a basal distance about 12.4 Å (Arp). Sheets of Arp seem to be united with micrometric size. Yet, for H₃-Sm TEM micrograph shows multiphase systems (42.1 Å, 32 Å, 22 Å and 14.6 Å) consisting of both curved and randomly intercalated layers with some regularly and flat layer occurred only in a small area (Fig. 6).

3.1.4. Specific surface area (S_{BET}) and cation exchange capacity (CEC)

Specific surface area (Fig. 7), pore volume, and CEC of all samples are presented in Table 3.

Surface area drops dramatically from 72.2 cm³ g⁻¹ (Arp) to 1.83 cm³ g⁻¹ (H₃-Sm), pore volume for organosmectite decreases with the increasing surfactants loaded. This suggests that interparticle pores of smectite are covered and the interlamellar spaces are blocked, lead to inhibition of the passage of N₂ molecules. This is distinctive by the decrease of pores volumes by HDTMA increasing density. Micropores surface area (S_{pp}) and micropores volumes (v_{pp}) were annulled after organophilic modification.

Cation exchange capacity (CEC) decreases with the increase of HDTMA density, it shifts from 91 meq/100 g (Na-clay) to 11 meq/100 g (H₃-Sm).

From XRD, CEC and S_{BET} results, it can be estimated that HDTMA⁺ occupies interlayer space, via cation exchange with Na⁺ interlayer, and the surface adsorption sites. Proposed mechanisms of HDTMA interaction can be summarized by the following presentation (Fig. 8).

3.1.5. Masse titration

Mass titration data performed at 0.01M NaCl concentrations are presented in Fig. 9. PZC of each sample was estimated (Table 4). Results show that the PZC of organo-modified smectite was displaced to the basic zone compared to that of Na-smectite (Arp). pH_{PZC} increases from 6.5 to 8.9. Organosmectites develop more positives charges than unmodified clay (Arp). Hydrophobic surface properties were obtained for organosmectites. Similar remarks were reported in many previous studies [38,41,42].

3.1.6. Optical properties

The results are shown in Fig. 10a. In this study, we give only the example of organophilic smectite H₃-Sm. Also, the band gap energy of H₃-Sm can be calculated from the optical absorption edge onset (λ) of reflectance spectrum by the following equation:

$$E \text{ (eV)} = 1240 / \lambda \text{ (nm)} \quad (6)$$

where λ is the absorption edge and E is the band gap energy of synthesized sample. As-synthesized organophilic smectite obtains a steep absorption edge which lies between 320 and 360 nm. The band gap energy is calculated to be 3.35 eV (Fig. 10b). Additionally, no other transition is observed in the spectrum which further confirms the purity of synthesized organophilic smectite.

3.2. CR removal studies

3.2.1. Adsorption isotherms

Fig. 11a shows the amounts of adsorbed quantities of CR at equilibrium (q_e) vs. equilibrium CR concentration (C_e).

According to Giles [43] classification, adsorption isotherms of CR with Arp and H₃-Sm are of type L and H respectively.

Results show that the maximum adsorption capacities of CR adsorbed onto organosmectite (experimental q_e ; $q_{e,exp}$ = 687 mg·g⁻¹) is larger than that on purified smectite ($q_{e,exp}$

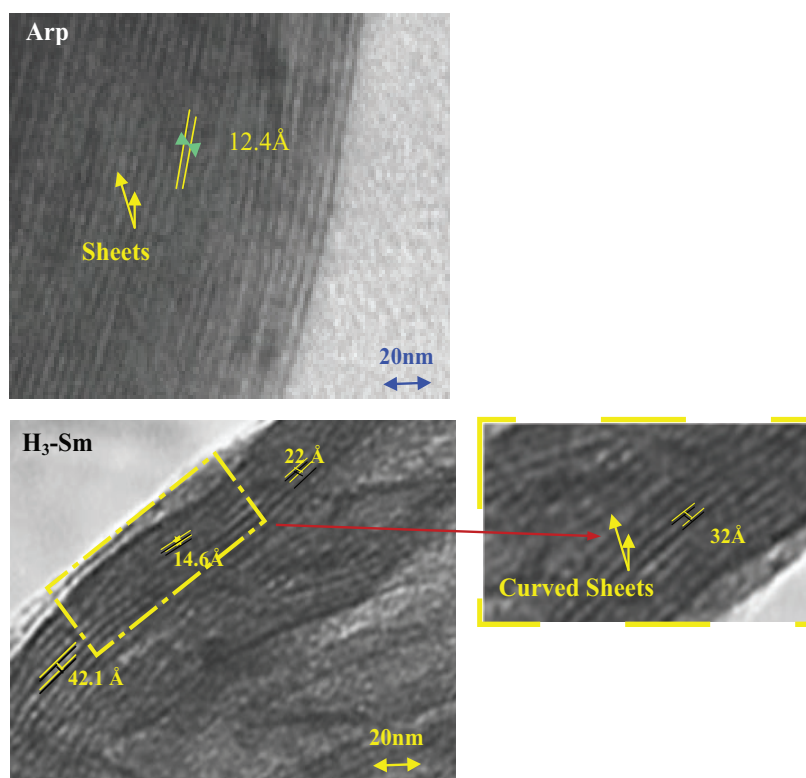


Fig. 6. TEM micrographs of Arp and H₃-Sm.

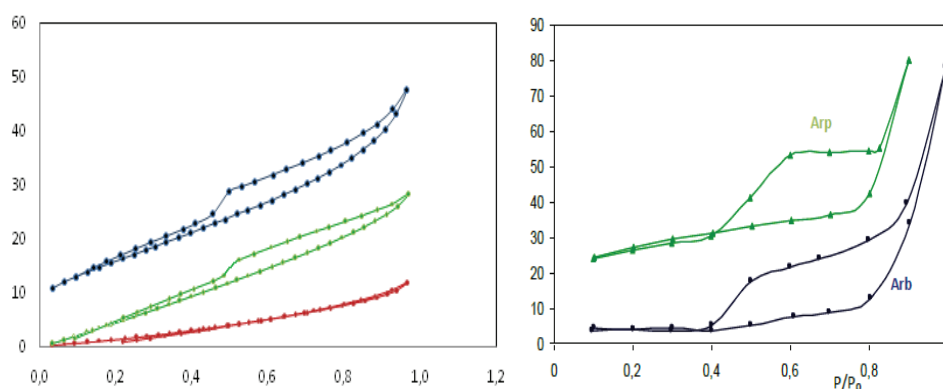


Fig. 7. Nitrogen adsorption-desorption isotherms at 77K of adsorbents.

Table 3
Characterization results of Arb, Arp and organosmectites

| Samples | S _{BET} (m ² g ⁻¹) | S _{HP} (m ² g ⁻¹) | V _P (cm ³ g ⁻¹) | V _{HP} (cm ³ g ⁻¹) | CEC (meq/100 g) |
|--------------------|---|--|--|---|--------------------|
| Arb | 34.98 | 5.8 | 0.085 | – | 66.9 |
| Arp | 72.2 | 8.7 | 0.138 | 0.014 | 89 |
| H ₁ -Sm | 12 | – | 0.091 | – | 38 |
| H ₂ -Sm | 4.25 | – | 0.007 | – | 21 |
| H ₃ -Sm | 1.83 | – | 0.001 | – | 11 |

= 285 mg·g⁻¹); there was a relatively high affinity between H₃-Sm and CR anion (which is completely adsorbed, we have noted a total discoloration of CR solution) this could be due to the high amount of surfactant loading on the surface of the smectite particles, which could results in increasing amount of positives charged sites and eventually facilitates the attraction towards the negatively charged dye molecules.

From the characterization studies of Arp and H₃-Sm the mechanisms of adsorbed CR are suggested. Arp has mainly electrostatic attraction between the negatively charged groups (–SO₃⁻) in CR and hydrated cation in interlayer space of the clay and/ or the positively charged surface

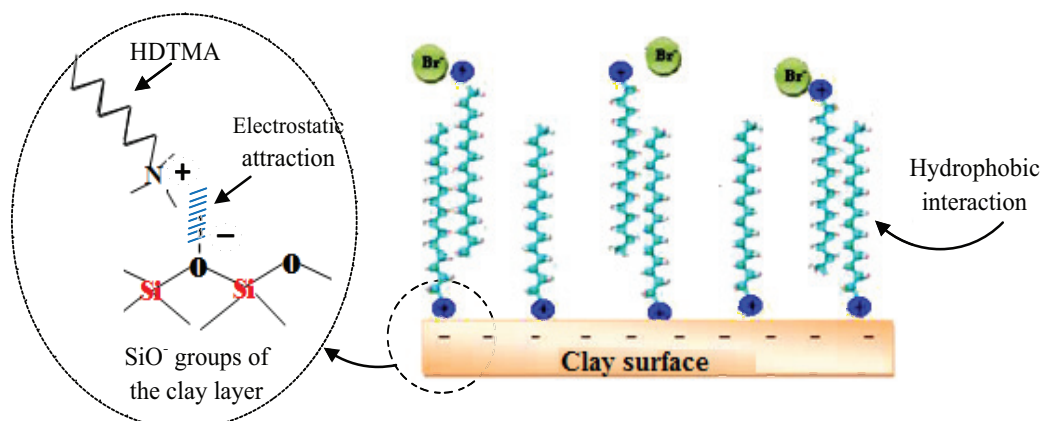


Fig. 8. Interaction of surfactant ion with Arp.

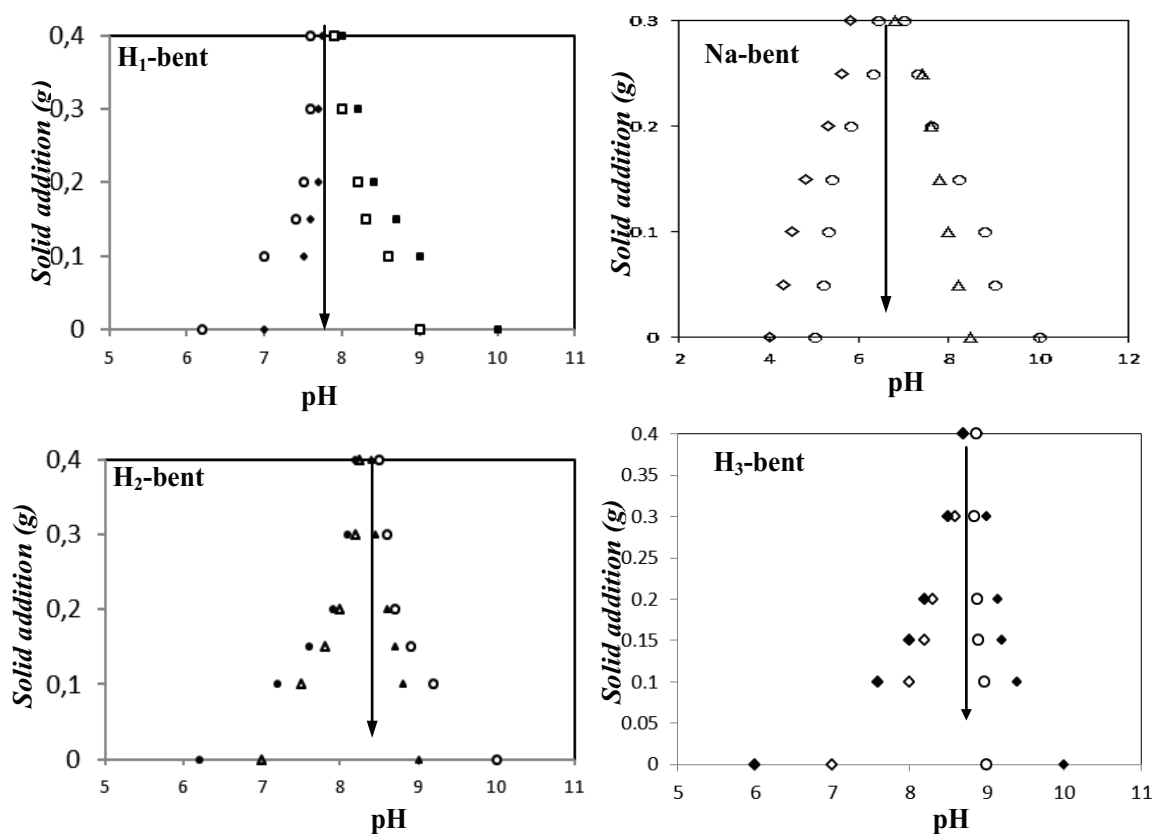


Fig. 9. Mass titration curves of Arp and organosmectites.

Table 4
pH of PCN data estimated by Mass titration method

| Samples | pH _{PZC} |
|--------------------|-------------------|
| Arp | 6.5 |
| H ₁ -Sm | 7.8 |
| H ₂ -Sm | 8.4 |
| H ₃ -Sm | 8.9 |

sites and therefore an increase in d-spacing is observed in XRD pattern (Fig. 5).

Generally, depending on the silica structure and the pH of the solution, the net surface charge can be either positive or negative. Adsorption of cations was favoured at $\text{pH} > \text{pH}_{\text{PZC}}$ while the adsorption of anions was favoured at $\text{pH} < \text{pH}_{\text{PZC}}$ [44].

The final pH of each solution was measured; it is equal to 6.3 and 6.7 for Arp and H₃-Sm respectively. These values are less than pH_{PZC} of each adsorbent which promotes

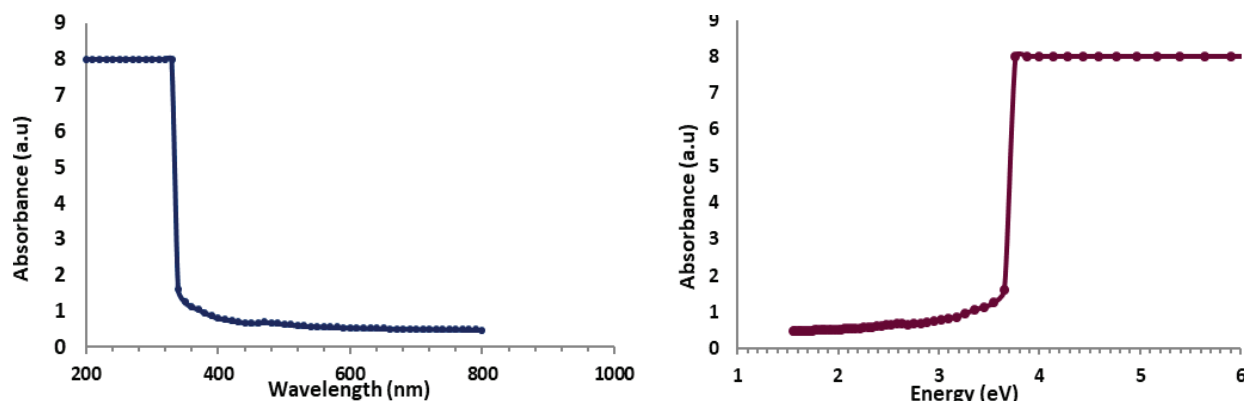


Fig. 10 (a). UV-Vis diffuse reflection spectra of H₃-Sm, (b): band gap determination of H₃-Sm.

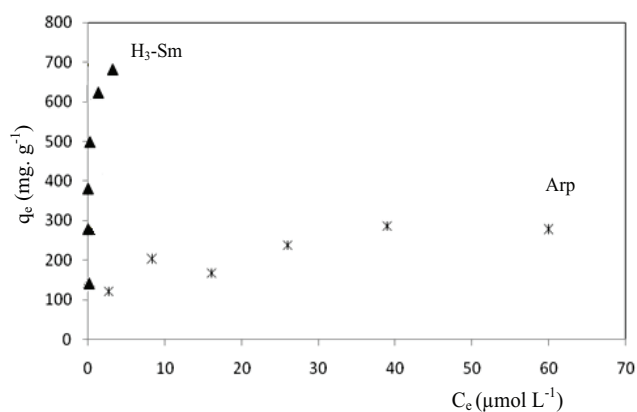


Fig. 11(a). Adsorption isotherms of CR by Arp and H₃-Sm.

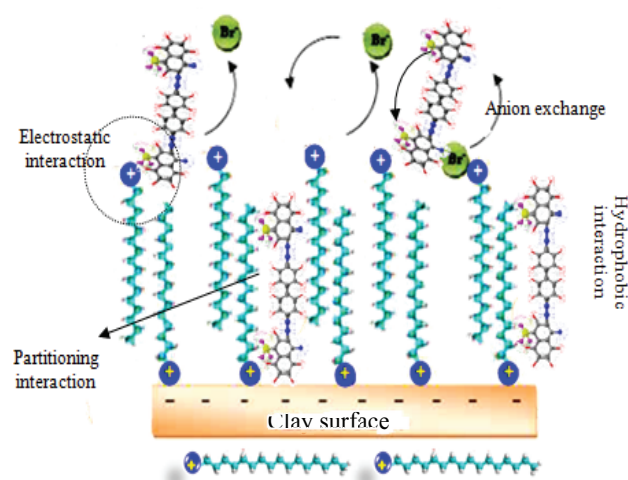


Fig. 11 (b). Adsorption mechanism of CR retention onto H₃-Sm.

the adsorption of this anionic dye. The Arp adsorption isotherm (type L) suggest a monolayer adsorption [43].

The adsorption behavior of CR onto H₃-Sm can be due to the positive charge on the H₃-Sm sheets (pH_{PZC} = 8.9) and thereby suggests electrostatic attraction between the negatively charged -SO₃⁻ of anion dye and the cationic surfactant

Table 5

Langmuir and Freundlich isotherm parameters for the CR adsorption onto Arp and H₃-Sm

| Langmuir isotherm | | | | Freundlich isotherm | | | |
|-------------------------------------|-------------------------------------|------------------------------|-------|---------------------|-------|-------|-------|
| <i>Arp</i> | | | | | | | |
| $q_{e,cal}$ (g g ⁻¹) | $q_{e,exp}$ (g·g ⁻¹) | K_L (g ⁻¹ L) | R^2 | R_L | K_F | 1/n | R^2 |
| 0.312 | 0.285 | 213.66 | 0.967 | 0.112 | – | 0.270 | 0.843 |
| <i>H₃-Sm</i> | | | | | | | |
| 0.671 | 0.687 | 372.56 | 0.996 | 0.037 | – | 0.118 | 0.428 |

head groups (-N⁺(CH₃)₃), which was proved by the type of adsorption curve, type H₁, that generally is the result of the dominance of strong ionic adsorbate-adsorbent interactions. In addition, H₃-Sm constructs an organic phase (with hydrophobic properties) that provides a partition medium for CR molecules which adhere to the adsorbed surfactant by van der Waals forces. Anion exchange with Br⁻ and anionic CR molecules can also be estimated (d-spacing increase after CR adsorption (Fig. 6)). Therefore, the synergetic effects of partitioning, electrostatic attraction, anion exchange and van der Waals forces effectively enhance the removal of anionic CR molecules from aqueous solution, causing a total discoloration of CR solution. Adsorption mechanism can be illustrated as follow (Fig. 11b).

The experimental data fit very well with the Langmuir model in view of the fact that correlation coefficient R² have a high value (Table 5). This model, suggests a monolayer adsorption process of CR with both adsorbents (Arp and H₃-Sm). Moreover, the similar values of the calculated $q_{e,cal}$ (calculated q_e) and the experimental values $q_{e,exp}$ (Table 5) verify the good conformity of this model.

Essential characteristics of Langmuir isotherm can be expressed in terms of a dimensionless constant separation factor R_L [45] that is given by the following equation:

$$R_L = \frac{1}{1 + K_L C_0} \quad (7)$$

The value of R_L indicates the shape of the isotherm which is: (i) unfavorable ($R_L > 1$), (ii) linear ($R_L = 1$), (iii) favorable

($0 < R_L < 1$), (iv) or irreversible ($R_L = 0$). From the R_L value (Table 5) the adsorption was a favorable process.

3.2.2. Effect of adsorption dose

The percentage of CR removal increased with the increase of Arp dosage (Fig. 12). 97.8% of CR was removed with 1 g of Arp and the red color of the aqueous solution greatly diminishes. However, with 0.1 g of H_3 -Sm total discoloration was reached (100% CR removal).

3.2.3. Effect of contact time

The plot of adsorption capacity vs. the contact time (Fig. 13) shows a fast removal of the dye from the beginning of the experiment afterward it proceeds at slower rate and finally gets to equilibrium which was attained for 60 min by Arp and 20 min by H_3 -Sm.

In order to examine the adsorption process of CR onto these adsorbents, pseudo-first order and pseudo-second order models are used to test the experimental data and to predict the mechanism involved in sorption process. The kinetics data were analyzed based on the regression coefficient R^2 , and the amount of dye removal at equilibrium.

The pseudo-first order model was suggested by [46], the linear form of this model was described by the following equation:

$$\ln(q_e - q_t) = \ln q_e - k_1 t \tag{8}$$

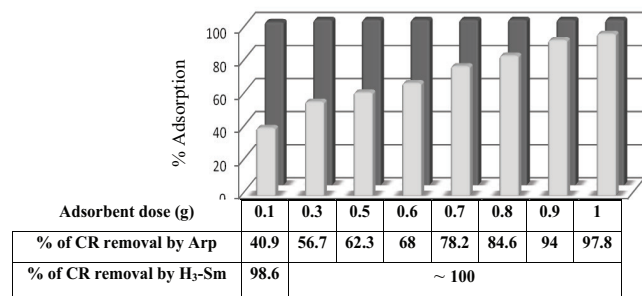


Fig. 12. Effect of adsorbent dose on the removal of CR (□ Arp, ■ H_3 -Sm).

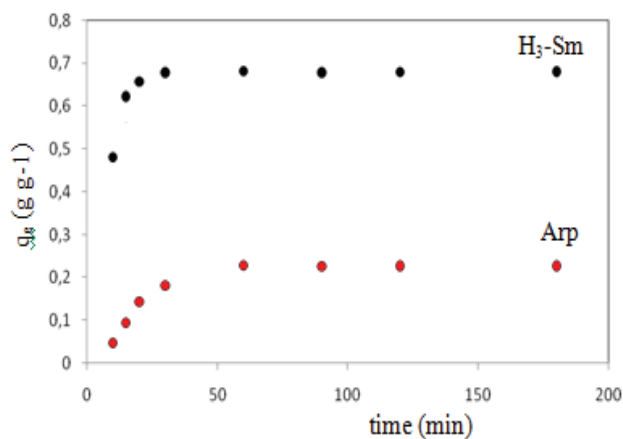


Fig. 13. Effect of contact time on CR removal by Arp and H_3 -Sm.

The validity of this model can be squared by linearized plot of $\ln(q_e - q_t)$ vs. t (figure not given).

The pseudo second order kinetic equation proposed by [47] based on the assumption that the adsorption follows second order chemisorption. The pseudo-second order can be expressed by the following equation:

$$\frac{t}{q_t} = \frac{1}{k_2 q_e^2} + \frac{t}{q_e} \tag{9}$$

This model can be squared by a linearized plot of $\frac{t}{q_t}$ vs. t (Fig. 14). The rate constant of pseudo second order adsorption and q_e are determined from the intercept and slope of the plot (Table 6).

We noted that q_e ($g \cdot g^{-1}$) and q_t ($g \cdot g^{-1}$) are the adsorbed amounts of CR at equilibrium and time t (min); k_1 (min^{-1}) and k_2 ($mg^{-1} g \cdot min^{-1}$) are the adsorption rate constants of the first order and the Pseudo-second-order equation respectively.

The correlation coefficients of the pseudo-first order are lower ($R^2 = 0.623$ (Arp), $R^2 = 0.564$ (H_3 -Sm)). Furthermore a large difference between the experimental ($q_{e,exp}$) and the calculated ($q_{e,cal}$) equilibrium adsorption capacity indicating a poor pseudo-first-order model fit to experimental data.

The high correlation coefficients ($R^2 > 0.99$) of the pseudo-second order kinetics and the $q_{e,cal}$ values agree with the experimental data suggest that this model fit with adsorption data and supports the hypothesis [48] that the rate limiting-step of dye onto adsorbents may be chemical sorption or chemisorption as reported by [49].

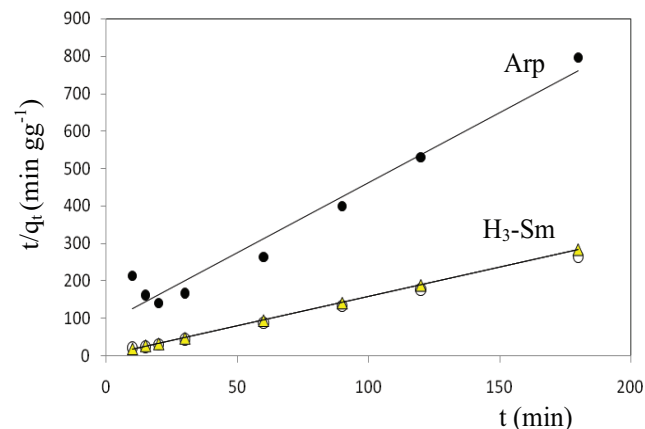


Fig. 14. Pseudo-second order for CR adsorption onto Arp and H_3 -Sm.

Table 6
Pseudo-second-order and pseudo-first order parameters for CR removal by Arp and H_3 -Sm

| Pseudo-second-order | | | Pseudo-first-order | |
|---|----------------------------------|-------|----------------------------------|-------|
| K_2 ($g \cdot g^{-1} \cdot min^{-1}$) | $q_{e,cal}$ ($g \cdot g^{-1}$) | R^2 | $q_{e,cal}$ ($g \cdot g^{-1}$) | R^2 |
| Arp | | | | |
| 0.156 | 0.267 | 0.993 | 0.185 | 0.623 |
| H_3 -Sm | | | | |
| 3.406 | 0.682 | 0.999 | 0.580 | 0.564 |

3.2.4. Study of the suitability of Arp as adsorbent for the treatment of real effluent from a Tunisian textile industry

The results of the adsorbent dose effect onto CR removal from aqueous solutions studies, show that the concentration of CR was reduced in the order of 97.8 % with an initial dye concentration of 69.66 mg·L⁻¹ and adsorbent Arp dose of 1 g, this result gives rise to the use of Arp as adsorbent for textiles effluent treatment containing anionic dye and avoid the use of organoclay containing chemicals compound.

Therefore, sample of wastewater from Tunisian textile industry (installed in the North East of Tunisia) specialized in finishing of cotton fabric; washing and dyeing (using CR as molecule dye) was collected to be treated with Arp as adsorbent. The effluent was sampled at the process exit and therefore contains the chemical compounds used throughout the dyeing procedure. The additives used in this industry are presented in table 7 determined in our previous work [50].

To test the affinity of Arp as adsorbent for the collected effluent treatment, batch experiment was carried out using 5 g of Arp mixed with 50 mL of the considered effluent based on our previous study [50]. The mixer was agitated during 60 min at room temperature then centrifuged and the supernatant was analyzed. The main compositions of the effluent before and after treatment are summarized in Table 8.

After the treatment of the effluent with Arp their parameters values decrease, the pH of solution tended to reach a neutral value corresponding to acceptable value that can realise in aquatic medium (6.5 < pH < 8.5) [53]. DBO and DCO values respect the conditions for release in public hydrolic domain, yet not in aquatic environment because of high salinity. The treated water can be re-used for agriculture since it obeyed the norms for reuse in agriculture [54], it can be used for vegetation adabted to high salinity.

To avoid the transfer of pollution from aqueous medium to soil the adsorbents after dye adsorption will be treated by advance oxydation process such as Fenton oxydation. This

Table 7
Main characteristics of the additives used by the textile finishing industry

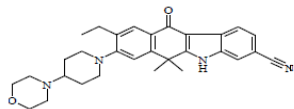
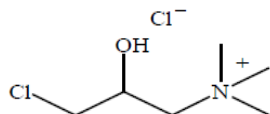
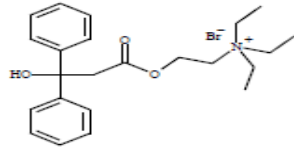
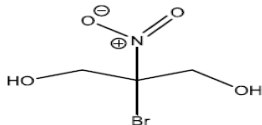
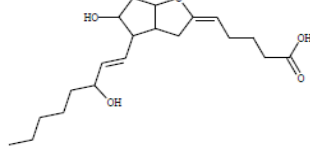
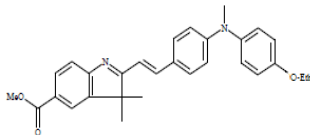
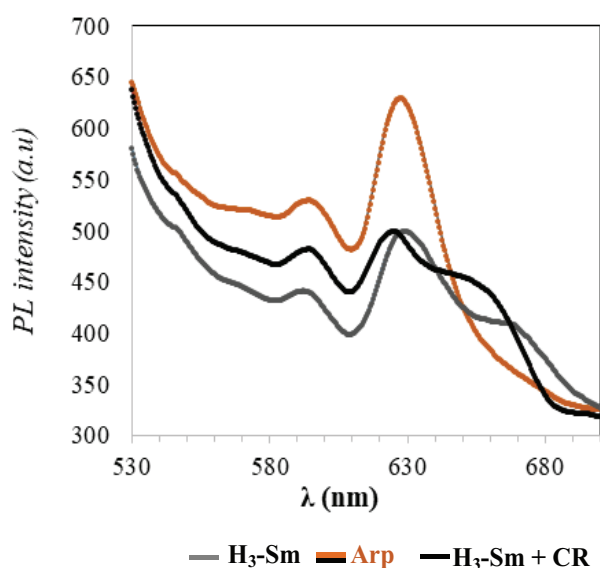
| Additifs | Structurals formula |
|---|---|
| <p>CHT Catalase Enzymatic auxiliary used for the destruction of residual peroxide after textile bleaching (C₃₀H₃₄N₄O₂ FW: 482.62 g mol⁻¹).</p> |  |
| <p>Kollasol Cationic surfactant composed of silicone mixed with higher alcohols. It acts as a degasser and penetration accelerator. Used for the cationisation of cellulose before dyeing with anionic dyes [51,52]. (C₆H₁₅Cl₂NO, FW: 188.12 g·mol⁻¹).</p> |  |
| <p>Meropan DPE Polycarboxylic acid with modified phosphonates, it has the role of a colloid protector (C₂₃H₃₂BrNO₃, FW: 449.90 g mol⁻¹).</p> |  |
| <p>Bactosol A bacterial enzyme compound used for cellulosic materials under acidic conditions; It improves the appearance of the surface, and helps in achieving a washed-out effect with fewer stones. (C₃H₆BrNO₄, FW: 199.98 g mol⁻¹)</p> |  |
| <p>Cotoblanc sel 200 Mélange d'un agent séquestrant et de polymères avec une affinité pour les colorants; il supprime les colorants réactifs non fixés sur les substrats cellulosiques. (C₂₀H₃₂O₅, FW: 352 g mol⁻¹)</p> |  |
| <p>Duralkan FSR A nitrogenous polycondensation product, it is formed of formaldehyde and free metal. It is a fixing agent. (C₂₉H₃₀N₂O₃, FW : 454 g mol⁻¹)</p> |  |

Table 8

The main compositions and characteristic of the effluent before and after treatment with Arp as adsorbent

| Effluents composition before treatment | | | | | | | |
|--|---|-----------------------------------|---|--|---|---|---|
| pH | Conductivity ($\mu\text{S cm}^{-1}$) | Salinity (g L^{-1}) | DBO_5 ($\text{mg O}_2 \text{L}^{-1}$) | DCO ($\text{mg O}_2 \text{L}^{-1}$) | Pt^* (mg L^{-1}) | N_t^{**} (mg L^{-1}) | SM^{***} (mg L^{-1}) |
| 11.3 | 7530 | 4.2 | 190 | 311 | 6.6 | 33 | 140 |
| Effluents composition after treatment | | | | | | | |
| 6.8 | 1405 | 3.4 | 6 | 62 | **** | **** | **** |

*phosphorus total, **total nitrogen, ***suspended matter

Fig. 15. Fluorescence emission spectra of Arp, $\text{H}_3\text{-Sm}$ before and after CR dye adsorption at an excitation wavelength $\lambda_{\text{ext}} = 498 \text{ nm}$.

investigation in our previous work and results show a total removal of dye and we regenerate the adsorbent safely [55].

3.2.5. Fluorescence study of $\text{H}_3\text{-Sm}$ before and after CR dye adsorption

The PL spectra of purified smectite Arp, $\text{H}_3\text{-Sm}$ before and after Congo red adsorption are carried out on exciting the sample at 498 nm at room temperature. As commonly known, this technique was used to confirm the electron hole recombination rate and behavior of photogenerated electron hole pairs [56]. In our case, we try to valorize the residue solid obtained after adsorption process (Congo red loaded in organo-smectite $\text{H}_3\text{-Sm}$). Obtained results are illustrated in Fig. 15. It can be seen that both unmodified smectite Arp and $\text{H}_3\text{-Sm}$ exhibit two emission peaks at 628 nm and 594 nm. But, Arp shows the strong and luminous emission peaks and the low intensity broad emission peak observed for $\text{H}_3\text{-Sm}$. Also, this organo-smectite shows an additional emission peak at 670 nm that is otherwise absent in purified smectite. This peak is the characteristic peak of HDTMA surfactant in the interlayer space of Arp.

The emission characteristics of $\text{H}_3\text{-Sm}$ before and after CR dye adsorption are differentiated by the position of their

emission peaks. After the adsorption of CR dye, emission peaks at 628 nm and 670 nm shifted slightly to the lower value of wavelength 626 nm and 658 nm, respectively. These results indicate that the intercalation of Smectite by HDTMA could effectively suppressed recombination rate of electron-hole pairs, also in the case of CR dye adsorption. Thus, it can be concluded that the appreciable low rate recombination ensure better photocatalytic performance [57] and these materials can be used in many application such as photocatalytic field.

4. Conclusion

Organosmectite prepared with HDTMA equivalent to 3 CEC has 8.9 pH_{PZC} and high values of basal interlayer spaces due to different surfactant arrangement, which have given it a heterogeneous structure. These properties affect the adsorption capacities of this adsorbent for organic dye pollutant such as CR by forming more hydrophobic partition medium. $\text{H}_3\text{-Sm}$ adsorb more CR (100%) than Arp with only 100 mg, yet Arp reach this rate with 1000 mg. The adsorption data of CR fit well with pseudo-second order kinetic model and the Langmuir model. The adsorption mechanism in case of Arp, is mainly based onto electrostatic attraction between the negatively charged groups ($-\text{SO}_3^-$) in CR and hydrated cation in interlayer space of the clay and/ or the positively charged surface sites. In case of $\text{H}_3\text{-Sm}$, adsorption mechanism is due to the effects of partitioning, electrostatic attraction, anion exchange and van der Waals forces, which effectively enhance the removal of anionic CR molecules from aqueous solution, causing a total discoloration of CR solution.

Optical and luminescence property of Arp and $\text{H}_3\text{-Sm}$ have been studied, results show that the complex organo-smectite after CR dye adsorption can be used in photocatalytic field.

Based onto the results concerning the effect of adsorption dose onto CR removal, Arp can be used as adsorbent for textiles effluent treatment containing anionic dye and avoid the use of organoclay containing chemicals compound. Result shows that the textile wastewater treated in this work with Arp can be re-used for agriculture for vegetation adapted to high salinity.

References

- [1] S. Pannuzzo, A. Serre, Traiter l'eau et les effluents industriels par les techniques membranaires et d'autres techniques couplées, L'eau, l'industrie, les nuisances., 235 (2000)123–128.

- [2] N. Erdumlu, B. Ozipek, G. Yilmaz, Z. Topatan, Reuse of effluent water obtained in different textile finishing processes, *Autex Res J.*, 12(1) (2012) 23–28.
- [3] S.S. Patil, V.M. Shinde, Biodegradation studies of aniline and nitrobenzene in aniline plant wastewater by gas chromatography. *Env. Sci. Tech.*, 22(10) (1988) 1160–1165.
- [4] M. Neamtu, A. Yediler, I. Siminiceanu, M. Macoveanu, A. Ketrup, Decolorization of disperse red 354 azo dye in water by several oxidation processes—a comparative study, *Dyes Pigm.*, 60(1) (2004) 61–68.
- [5] P.J. Halliday, S. Beszedits, Color removal from textile mill wastewaters, *Can. Tex. J.*, 103 (1986) 78–84.
- [6] N. Atar, A. Olgun, Removal of basic and acid dyes from aqueous solutions by a waste containing boron impurity, *Desalination*, 249 (2009) 109–115.
- [7] C. Yenikaya, E. Atar, A. Olgun, N. Atar, S. İlhan, F. Çolak, Biosorption study of anionic dyes from aqueous solutions using *Bacillus amyloliquefaciens*, *Eng. Life Sci.*, 10(3) (2010) 233–241.
- [8] N. Atar, A. Olgun, Removal of acid blue 062 on aqueous solution using calcinated colemanite ore waste, *J. Hazard. Mater.*, 146(1–2) (2007) 171–179.
- [9] A. Olgun, N. Atar, Equilibrium and kinetic adsorption study of Basic Yellow 28 and Basic Red 46 by a boron industry waste, *J. Hazard. Mater.*, 161(1) (2009) 148–156.
- [10] M.S. Onyango, T.Y. Leswif, A. Ochieng, D. Kuchar, F.O. Otieno, H. Matsuda, Breakthrough analysis for water defluoridation using surface-tailored zeolite in a fixed bed column, *Indust. Eng. Chem. Res.*, 48(2) (2008) 931–937.
- [11] E. Lorenc-Grabowska, G. Gryglewicz, Adsorption characteristics of Congo Red on coal-based mesoporous activated carbon, *Dyes Pigm.*, 74(1) (2007) 34–40.
- [12] M.S. Onyango, J. Kittinya, N. Hadebe, V.O. Ojijo, A. Ochieng, Sorption of melanoidin onto surfactant modified zeolite, *Chem. Indust. Chem. Eng. Quart.*, 17(4) (2011) 385–395.
- [13] A. Berez, G. Schäfer, F. Ayari, M. Trabelsi-Ayadi, Adsorptive removal of azo dyes from aqueous solutions by natural bentonite under static and dynamic flow conditions, *Int. J. Environ. Sci. Technol.*, 13(7) (2016) 1625–1640.
- [14] M. Alkan, S. Çelikçapa, S.Ö. Demirba, Removal of reactive blue 221 and acid blue 62 anionic dyes from aqueous solutions by sepiolite, *Dyes Pigm.*, 65(3) (2005) 251–259.
- [15] R.G. Harris, J.D. Wells, B.B. Johnson, Selective adsorption of dyes and other organic molecules to kaolinite and oxide surfaces, *Colloids Surf. A: Physicochem. Eng. Aspects.*, 180(1–2) (2001) 131–140.
- [16] R.S. Juang, S.H. Lin, K.H. Tsao, Mechanism of sorption of phenols from aqueous solutions onto surfactant-modified montmorillonite, *J. Colloid. Interf. Sci.*, 254(2) (2002) 234–241.
- [17] B. Erdem, A. Özcan, Ö. Gök, A.S. Özcan, Immobilization of 2, 2'-dipyridyl onto bentonite and its adsorption behavior of copper (II) ions, *J. Hazard. Mater.*, 163(1) (2009) 418–426.
- [18] Y.H. Shen, Preparations of organobentonite using nonionic surfactants, *Chemo.*, 44(5) (2001) 989–995.
- [19] A.S. Ozcan, B. Erdem, A. Ozcan, Adsorption of Acid Blue 193 from aqueous solutions onto Na-bentonite and DTMA-bentonite, *J. Colloid. Interf. Sci.*, 280(1) (2004) 44–54.
- [20] D.C. Rodriguez-Sarmiento, J.A. Pinzon-Bello, Adsorption of sodium dodecylbenzene sulfonate on organophilic bentonites, *Appl. Clay Sci.*, 18(3–4) (2001) 173–181.
- [21] L. Zhu, Y. Su, Benzene vapor sorption by organobentonites from ambient air, *Clays Clay Miner.*, 50(4) (2002) 421–427.
- [22] E. Manias, A. Subbotin, G. Hadziioannou, G. Ten Brinke, Adsorption-desorption kinetics in nanoscopically confined oligomer films under shear, *Molec. Phys.*, 85(5) (1995) 1017–1032.
- [23] J. Wu, M.M. Lerner, Structural, thermal, and electrical characterization of layered nanocomposites derived from sodium-montmorillonite and polyethers, *Chem. Mats.*, 5(6) (1993) 835–838.
- [24] S. Xu, G.Y. Liu, Nanometer-scale fabrication by simultaneous nanoshaving and molecular self-assembly, *Langmuir.*, 13(2) (1997) 127–129.
- [25] H.V. Olphen, An introduction to clay colloid chemistry, for clay technologists, geologists, and soil scientists (No. 04; QD549, O5.), (1963).
- [26] M.K. Purkait, A. Maiti, S. Dasgupta, S. De, Removal of congo red using activated carbon and its regeneration, *J. Hazard. Mater.*, 145(1–2) (2007) 287–295.
- [27] G. Maeder, J.L. Lebrun, D. David, R. Caplain, Méthodes usuelles de caractérisation des surfaces. D. David et R. Caplain (Eds.), Eyrolles, Paris, 1988, 248 p.
- [28] F. Bergaya, M. Vayer, CEC of clays: measurement by adsorption of a copper ethylenediamine complex, *Appl. Clay Sci.*, 12(3) (1997) 275–280.
- [29] J.S. Noh, J.A. Schwarz, Estimation of the point of zero charge of simple oxides by mass titration, *J. Colloid. Interf. Sci.*, 130(1) (1989) 157–164.
- [30] I. Langmuir, The adsorption of gases on plane surfaces of glass, mica and platinum, *J. Amer. Chem. Soc.*, 40(9) (1918) 1361–1403.
- [31] H. Freundlich, Über die adsorption in lösungen, *Zeitschrift für physikalische Chemie.*, 57(1) (1907) 385–470.
- [32] F. Bergaya, M. Vayer, CEC of clays: measurement by adsorption of a copper ethylenediamine complex, *Appl. Clay Sci.*, 12(3) (1997) 275–280.
- [33] S. Liang, X. Guo, N. Feng, Q. Tian, Isotherms, kinetics and thermodynamic studies of adsorption of Cu^{2+} from aqueous solutions by $\text{Mg}^{2+}/\text{K}^{+}$ type orange peel adsorbents, *J. Hazard. Mater.*, 174(1–3) (2010) 756–762.
- [34] C. Liu, H. Li, C.T. Johnston, S.A. Boyd, B.J. Teppen, Relating clay structural factors to dioxin adsorption by smectites: molecular dynamics simulations, *Soil Sci. Soc. Am. J.*, 76(1) (2012) 110–120.
- [35] G. Lagaly, Layer charge heterogeneity in vermiculites, *Clays Clay Miner.*, 30(3) (1982) 215–222.
- [36] S.Y. Lee, S.J. Kim, Delamination behavior of silicate layers by adsorption of cationic surfactants, *J. Colloid. Interf. Sci.*, 248(2) (2002) 231–238.
- [37] S.Y. Lee, S.J. Kim, Expansion characteristics of organoclay as a precursor to nanocomposites, *Colloids Surfaces A: Physicochem. Eng. Aspects.*, 211(1) (2002) 19–26.
- [38] G.E. Boyd, L.S. Myers Jr, A.W. Adamson, The exchange adsorption of ions from aqueous solutions by organic zeolites. III. Performance of deep adsorbent beds under non-equilibrium conditions, *J. Am. Chem. Soc.*, 69(11) (1947) 2849–2859.
- [39] H.P. He, J.G. Guo, J.X. Zhu, C. Hu, ^{29}Si and ^{27}Al MAS NMR study of the thermal transformations of kaolinite from North China, *Clay Miner.*, 38(4) (2003) 551–559.
- [40] N. Hamdi, E. Srasra, Acid-base properties of organosmectite in aqueous suspension, *Appl. Clay Sci.*, 99 (2014) 1–6.
- [41] C. Namasivayam, D. Sangeetha, R. Gunasekaran, Removal of anions, heavy metals, organics and dyes from water by adsorption onto a new activated carbon from *Jatropha* husk, an agro-industrial solid waste, *Process Safety Env. Prot.*, 85(2) (2007) 181–184.
- [42] Z. Wu, I.S. Ahn, C.H. Lee, J.H. Kim, Y.G. Shul, K. Lee, Enhancing the organic dye adsorption on porous xerogels, *Colloids Surf A: Physicochem. Eng. Asp.*, 240(1–3) (2004) 157–164.
- [43] M. Duc, F. Gaboriaud, F. Thomas, Sensitivity of the acid-base properties of clays to the methods of preparation and measurement: 1. Literature review, *J. Colloid. Interf. Sci.*, 289(1) (2005) 139–147.
- [44] C.H. Giles, S.N. Nakhwa, Studies in adsorption. XVI The measurement of specific surface areas of finely divided solids by solution adsorption, *J. Chem. Tech. Biotech.*, 12(6) (1962) 266–273.
- [45] M.A. Khraisheh, Y.S. Al-Degs, W.A. McMinn, Remediation of wastewater containing heavy metals using raw and modified diatomite, *Chem. Eng. J.*, 99(2) (2004) 177–184.
- [46] S. Lagergren, Zur theorie der sogenannten adsorption gelöster stoffe, *Kungliga Svenska Vetenskapsakademiens, Handlingar*, 24(4) (1898) 1–39.
- [47] Y.S. Ho, G. McKay, The kinetics of sorption of basic dyes from aqueous solution by sphagnum moss peat, *Canad. J. Chem. Eng.*, 76(4) (1998) 822–827.
- [48] Y.S. Ho, J.C.Y. Ng, G. McKay, Kinetics of pollutant sorption by biosorbents, *Sep. Purif. Meth.*, 29(2) (2000) 189–232.

- [49] Y. Liu, Y.J. Liu, Biosorption isotherms, kinetics and thermodynamics, *Sep. Purif. Tech.*, 61(3) (2008) 229–242.
- [50] A. Nejib, D. Joelle, A. Fadhila, G. Sophie, T.A. Malika, Adsorption of anionic dye on natural and organophilic clays: effect of textile dyeing additives, *Desal. Water Treat.*, 54(6) (2015) 1754–1769.
- [51] A. Benhammou, A. Yaacoubi, L. Nibou, B. Tanouti, Adsorption of metal ions onto Moroccan stevensite: kinetic and isotherm studies, *J. Colloid. Interf. Sci.*, 282(2) (2005) 320–326.
- [52] J.P. Hobson, Physical adsorption isotherms extending from ultrahigh vacuum to vapor pressure, *J. Phys. Chem.*, 73(8) (1969) 2720–2727.
- [53] NT. 106.02, T. S.-B. o. J. b. t. M. o. t. N. E., Implementing the Tunisian Standard Concerning Wastewater Effluent Discharge in the Hydrous Medium.
- [54] NT 106.03, T. S.-D. o. D. M. t. D. o. J. b. t. M. o. t. N. E., Implementing the Tunisian Standard Concerning the Use of Treated Wastewater in Agriculture.
- [55] S. Khelifi, F. Ayari, A. Choukchou-Braham, D.B.H. Chehimi, The remarkable effect of Al-Fe pillaring on the adsorption and catalytic activity of natural Tunisian bentonite in the degradation of azo dye, *J. Porous. Mater.*, 1–12 (2017).
- [56] Y. Shi, Z. Yang, Y. Liu, J. Yu, Wang, J. Tong, Q. Wang, Fabricating a gC₃N₄/CuO_x heterostructure with tunable valence transition for enhanced photocatalytic activity, *RSC Adv.*, 6(46) (2016) 39774–39783.
- [57] R. Tanwar, S. Kumar, U.K. Mandal, Photocatalytic activity of PANI/Fe₀ doped BiOCl under visible light-degradation of Congo red dye, *J. Photochem. Photobio. A: Chemistry.*, 333 (2017) 105–116.